

Feasibility of Conductively-Cooled Superconducting Magnets in a Linac Cryomodule

S. Cheban, T. Khabiboulline, F. Lewis, R. Madrak, B. Niels,
V. Poloubotko, D. Sergatskov, I. Terechkine, T. Wokas

I. Introduction.

This note summarizes studies towards a possibility of using conductively-cooled superconducting magnets in linac cryomodules, including the one in development for the FNAL's PXIE test facility [1]. Using conduction cooling can result in significant simplification of cryomodule design and saving of longitudinal real estate, precious in front ends of high current superconducting RF linacs. Our first attempt to use conductively-cooled magnet, although helped to answer certain questions (see [2] for details), did not bring the temperature of the winding to the level that would ensure efficient use of superconducting strand. This R&D was set to better understand cooling by conduction in the cryomodule environment and to develop a guideline for development of hardware needed for implementation of this cooling technique in cryomodules of superconducting linacs. Finding the ways to lower the temperature of the winding was one of the major goals of this study. At higher temperature of the winding, a lower critical current density in the strand translates into a need for a bigger magnet to achieve required focusing strength. In turn, a bigger magnet has a higher level of the fringe magnetic field, and, hence, additional measured are needed to shield superconducting cavities from this field.

The first challenge of this R&D was to find a way to deliver current to test magnets in the Spoke Cavity Test Cryostat [2] used for this study as it neither had any provisions for high current feedthroughs, no was equipped with proper heat exchangers to intercept the heat flux coming through or generated by the leads. This part of work was successfully completed and is described in [3]. The second problem was to modify DAQ system of the test facility so that the additional temperature sensors could be added to the existing setup. This issue was resolved by finding a way to re-use existing connectors in the Test Cryostat, adding new connectors, and using a stand-alone DAQ system in addition to the standard one, existing as a part of the test facility.

Two superconducting magnets were used during this study, and several test setups were tried to obtain needed information about the temperature of the winding in each coil. Initially, the work started with an attempt to use an existing superconducting solenoid fabricated in 2005 as part of an R&D towards HINS Focusing Lens development. Later, as uncertainties in the interpretation of the temperature readings became obvious, a superconducting solenoid was made which was better suited to this R&D. The next sections of the note describe each test, methods of temperature measurements, and provide analysis of the results.

II. Test Magnet #1

Full description of the design and performance of the first superconducting solenoid used during this R&D (Fig. 1) can be found in [4] and [5]. During this stage of the R&D, a method of temperature measurement in the magnet’s winding was developed and tested. This method was based on the relation between the known properties of the strand used in the magnet and the measured magnet quench current at different levels of the external heating power. Information needed for evaluation of the magnet performance (that is the quench current) is provided below. Dimensions shown in this figure refer only to the winding; insulation thickness is not included.

Inner Diameter	61.2 mm
Outer Diameter	93.2 mm
Length	101 mm
Number of turns in the coil	2355.7
Coil resistance at 300 K	32.0 Ohm
Coil inductance (without collar) 150 mH	

The solenoid was wound using round, 0.808 mm (bare) diameter NbTi strand made by Sumitomo. Performance of the strand (the current sharing limit I_{cr} and the quench current I_q), measured in the FNAL TD Strand Test facility at 4.2 K, is shown in Table 1 compared with the parameterized strand performance model I_p [6]. A parameterized model of strand properties allows calculation of coil’s quench current at any temperature; this provides a mean to calculate the temperature of the strand if the quench current is measured.

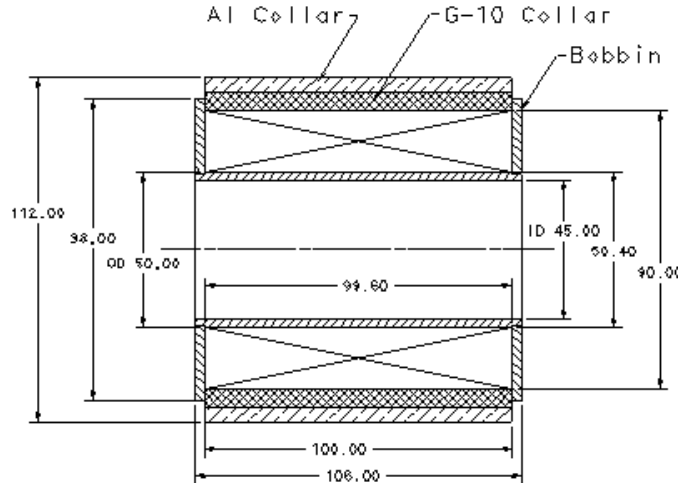


Fig. 1. Test magnet #1

Table 1. Sumitomo 0.808 mm strand performance at 4.2 K

B [T]	10	9	8	7	6	5	4	3	2	1	0
I_{cr} [A]	20	120	237	365	480	611	750	913	1150	1570	1700
I_q [A]	53	150	269	405	520	640	798	968	1218	1636	1741
I_p [A]		80	259	393	513	641	789	976	1234	1629	1690

Graphs in Fig. 2 compare the measured critical current of the strands at 4.2 K (red) with the one found using the parameterized model (blue).

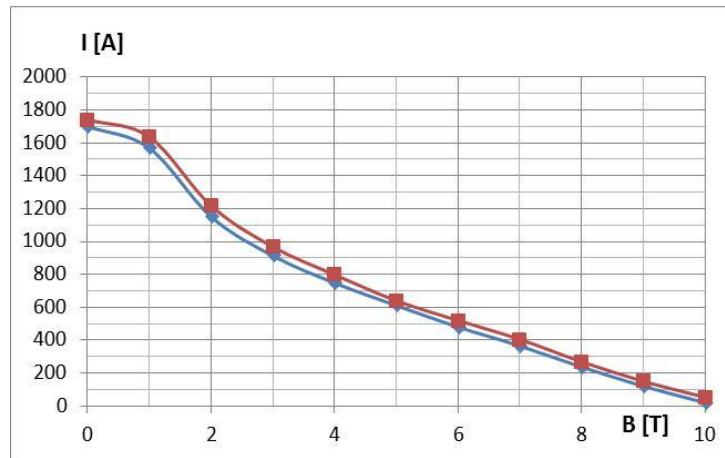


Fig. 2. Sumitomo 0.808 mm strand properties at 4.2 K.

The quench current in the solenoid reached the projected level: $I_q = 302.6$ A at 4.2 K [5]; the magnetic field in the center of the coil at the quench current was 7.04 T; maximum field in the winding reached 7.4 T. The maximum field on the strand can be evaluated using the expression

$$B_{str} [T] = 0.0244 \cdot I [A].$$

In Fig. 3, the load curve of the test coil is added to the traces of the strand performances for several temperatures. The crossing points in the graph establish correspondence between the strand temperature and the quench currents. For example, if the temperature is 6.5 K, we can expect quench at ~175 A; if it is 8 K, the quench current is only ~85 A.

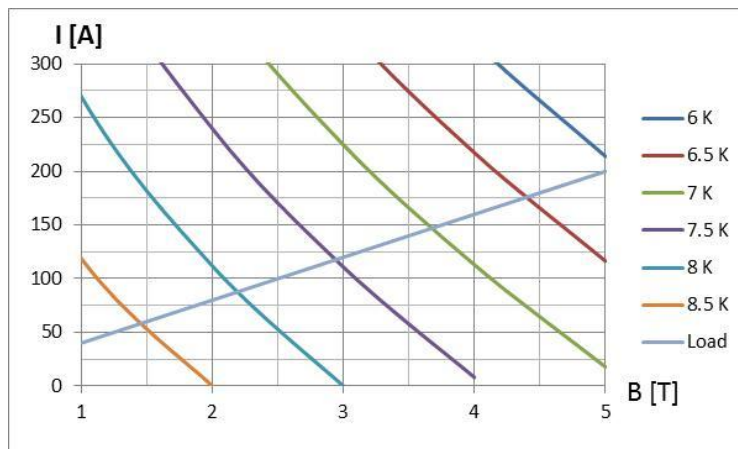


Fig. 3. Correspondence between the temperature and the quench current of the test coil #1

The solenoid was equipped with four heaters (4.9 Ohm MINCO-5160 Polyimide Heaters) mounted under the first layer of the winding; they were used during this test to change temperature at the location of the quench spot. The heaters were connected in series, so the total resistance was 19.6 Ohm at room temperature. At 4 K this resistance is lower by ~10%; the 17.8 Ohm resistance value was used to calculate the power generated by the heaters. The location of the heaters is illustrated in Fig. 4.



Fig. 4. Placement of heaters inside the winding of the magnet.

There were no temperature sensors embedded in the winding of this coil, so we needed to rely only on the sensors installed on the outer surface of the magnet during this stage of the R&D in our attempt to compare the readings of these sensors with the temperature calculated from the quench current measurements.

The test setup was changed several times during this R&D in an attempt to catch details of the temperature distribution in the winding, the heat flux patterns in the coil and in the fixture used to mount it in the cryostat. The maximum current available for the test also changed several times as the current lead performance was understood, a new way to deliver the current inside the cryostat was found and tested, and more powerful power supplies were employed.

The quench current of this magnet could not be reached without using the heaters. Nevertheless, indirect measurements showed that the temperature of the winding may be low enough to allow its effective use in the cryomodules. In Fig. 5, the extrapolation of the winding temperature found by calculations based on the quench current measurements (diamonds) to the level corresponding to the zero heating power is shown; the 4.75 K temperature is just slightly higher than the 4.65 K temperature of the LHe-cooled base plate where the magnet is installed, which was measured by CERNOX sensor.

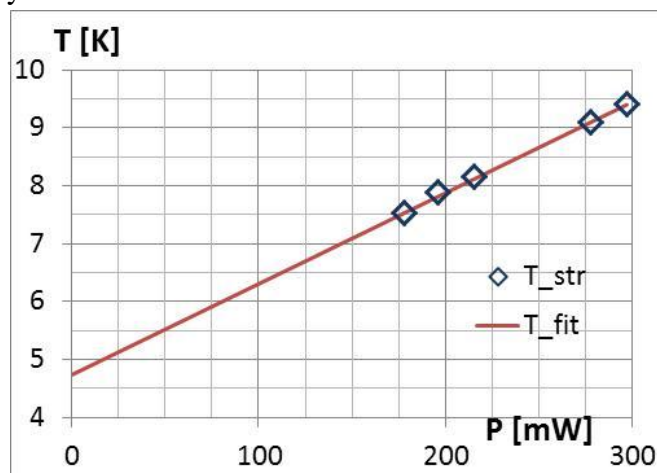


Fig. 5. Calculated temperature of the winding in the magnet #1 as a function of the heater power.

The deficiency of the indirect method in this particular case requiring extrapolation over a wide range of the heater power, forced us to fabricate a new test magnet with embedded temperature sensors. Due to limitation on the number of additional sensors in the test cryostat, only two sensors could be used, which were located in the middle of the first layer and in the middle of the last layer of the solenoid's winding. The new test coil is described in details in the next chapter.

III. Test Magnet #2

To reach the quench current in the new coil without using heaters, a thinner strand ought to be used; 0.5 mm NbTi strand provided by Oxford Instruments Inc. was used in this case. Table 2 compares the performance of the strand at 4.2 K with that specified by the vendor and with what parameterized strand performance predicts at 4.2 K.

Table 2. Strand performance comparison table

	B (T)	8	7	6	5	4	3	2	1	0
Sample #1	Ic (A)	98	151	202	255	308	367	451	621	826
Sample #2	Ic (A)		154	206	258	310	370	456	646	831
Specification	Ic (A)	94	134	173	213	252				
Parameterization	Ic (A)		126		207					

The coil parameters and expected performance are as follows:

- inner diameter of the winding is 48 mm;
- outer diameter is 99.6 mm;
- length of the coil is 109.8 mm;
- number of turns in the coil is 9954.

To reuse the hardware from the test of the coil #1, the compression ring in the magnet #2 was made to match the existing clamps: ID = 103.4 mm and OD = 110.1 mm. It was assembled with the coil's winding with the interference of 0.1 mm (by radius). The compaction factor of the winding is 0.68. The resistance of the winding at room temperature is 356 Ohm.

Fig. 6 shows a sketch of the magnet assembled on the base plate using clamps. The magnet is mounted on the cooling plate and equipped with a heater in the inner layer, similar to what was in the test magnet #1. The Cernox sensor in the inner layer (X60233 in the diagram in Fig. 9) was connected to the XN2 channel of the stand-alone DAQ; the sensor in the outer layer (X60232) was using the XN3 channel. It is necessary to note that the location of the temperature sensor in the inner layer does not coincide with the location of the heaters. If no heaters are activated, and assuming that the coil is properly trained, the quench spot in the coil is expected in the middle of the inner layer; it is above one of the heaters though, if a non-zero heater current is used. This feature of the setup will be developed further in this note.

This setup also included two radiation shields attached to the top halves of the clamps. The purpose of the shields is to protect the coil from an ambient heat leak we observed during the previous cooldown by redirecting this heat to the clamps; the two halves of the two clamps were thermally connected by strips of copper to improve thermal conductance to the heat sink.

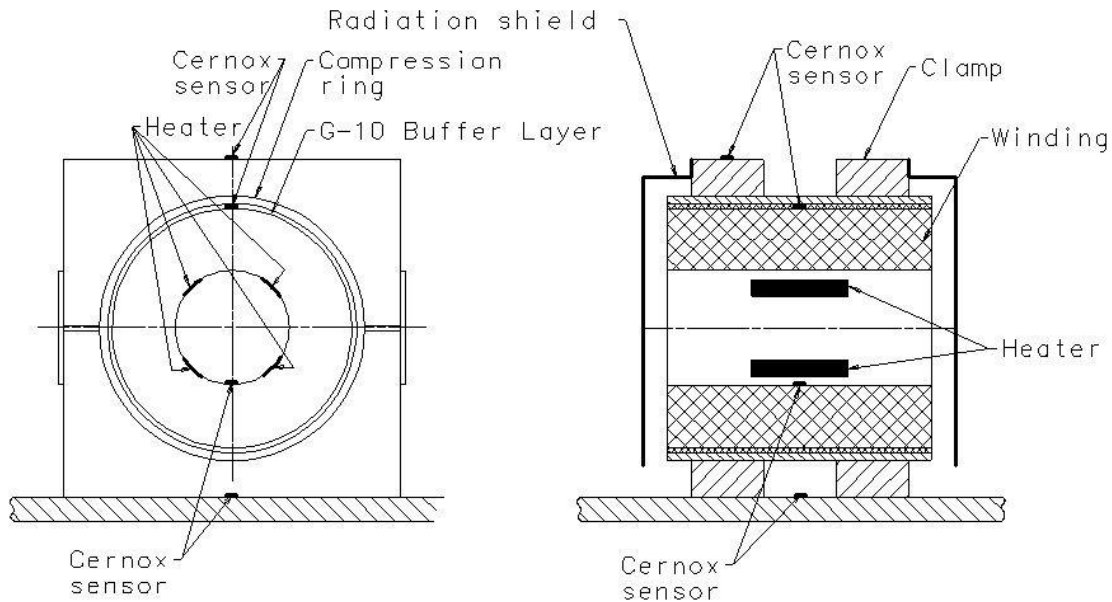


Fig. 6. Test magnet #2 and location of embedded instrumentation.

Maximum magnetic field on the winding can be expressed as a function of the current as

$$B [T] = 0.5 \cdot I [A].$$

By combining this expression with the parameterized performance of the strand at different temperatures, similar to what is shown in Fig. 3, we can find expected quench current of this coil at different temperatures of the strand (Fig. 7). It is well within the comfortable range of the power supply and the current leads. The linear dependence of the quench current on the strand temperature at $T > 5$ K will be used when the results are analyzed.

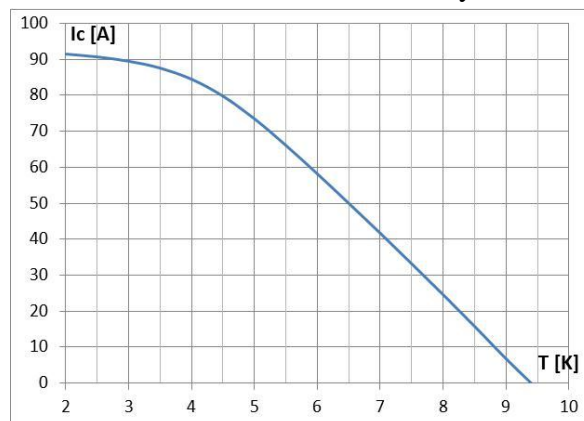


Fig. 7. Expected quench current of the new test coil at different temperatures of the strand

Because the magnet #2 was newly fabricated, it needed some training; Fig. 8 shows its training history. As the coil was cooled by conduction, the time constant of thermalization after a quench was substantial - ~20 min. The training was quite straightforward; the rate of the current rise affected the coil temperature though - some inconsistencies in the training history in Fig. 8 are results of the inductive heating when the current ramp rate was too high.

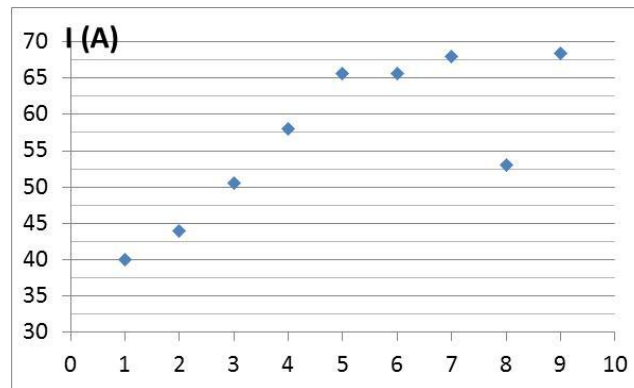


Fig. 8. Training history of the magnet #2

The maximum current reached during training was ~67 A. If we assume that the training was complete, this quench current corresponds to the temperature of the center of the first layer of the winding of ~5.5 K.

IV. Test setup & instrumentation

The latest version of the electrical and the cooling scheme of the test is shown in Fig. 9.

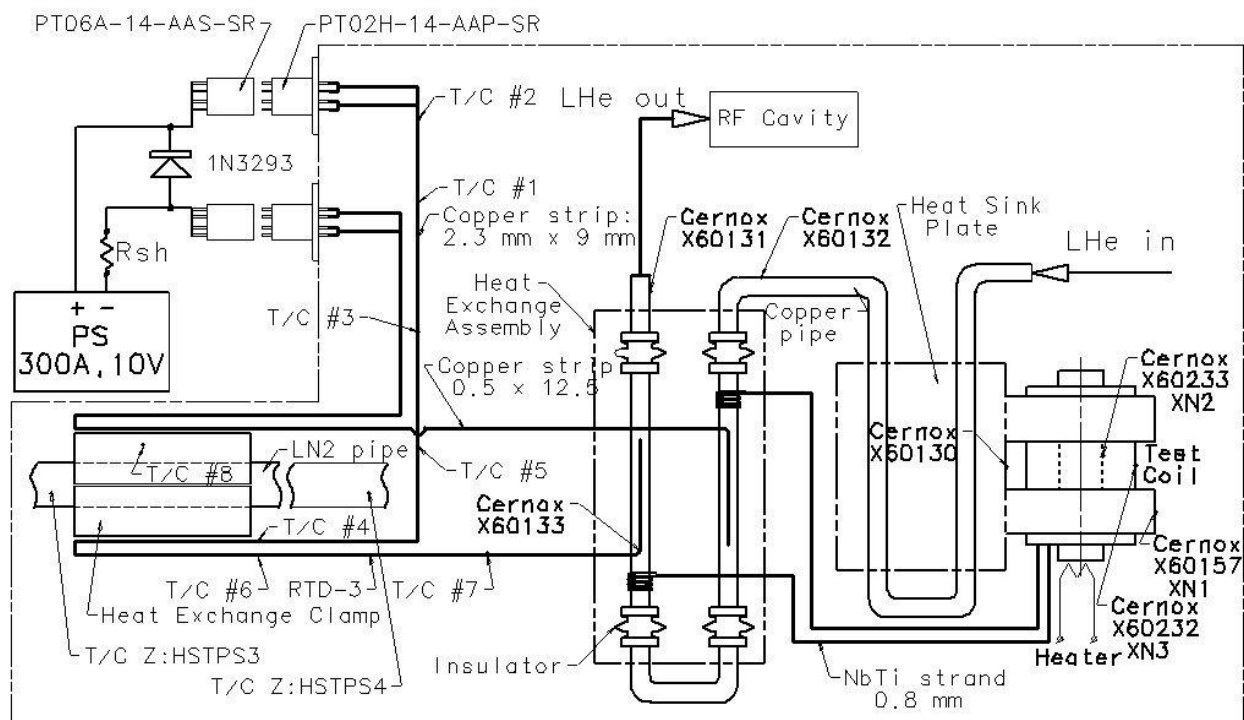


Fig. 9. Electrical and cooling scheme of the tests used with the test coil #2.

The magnet is fixed inside Al clamps and installed on the heat sink plate made of copper. The heat sink plate is cooled by liquid helium flowing through copper pipe brazed to the plate, which is mounted on insulating support post installed on the liquid Nitrogen (80 K) shield. Each current lead consists of two sections. The high-temperature section extends from the feed-through to the LN2 heat sink; it is made of annealed oxygen-free copper, 1.73 m long, and have $9 \times 2.3 \text{ mm}^2$

cross-section. The low-temperature section is connecting the LN2 heat sink with the LHe heat sink; it is 0.65 m long with $12.7 \times 0.51 \text{ mm}^2$ cross-section area.

Superconducting current leads of the magnet are connected to the low temperature section of the current leads at the LHe heat exchanger. Description of both heat exchangers of the current lead assembly is made in [3].

A CAD rendering of the setup and corresponding photos are shown in Fig. 10 and Fig. 11.

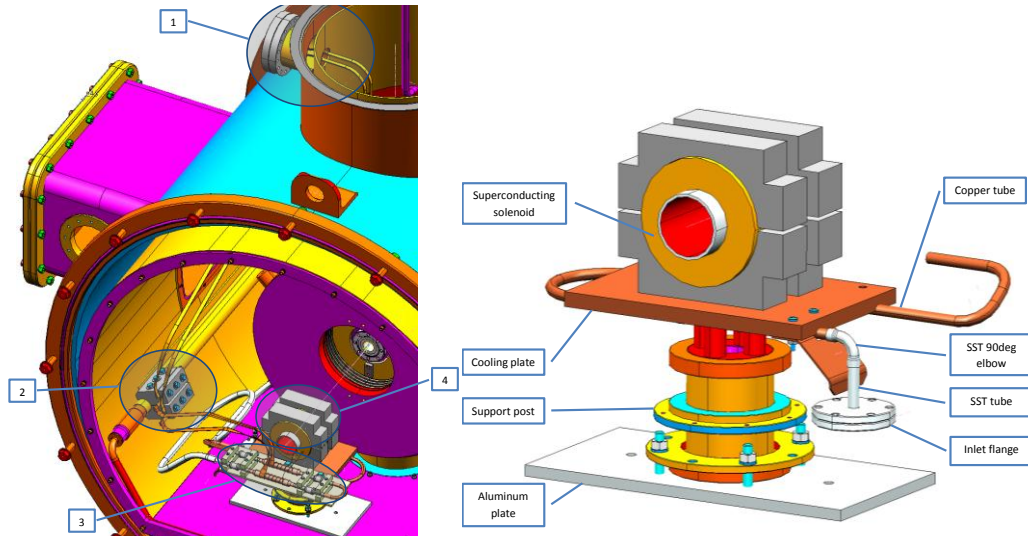


Fig. 10. Cryostat with mounted current leads, heat exchangers, and the magnet

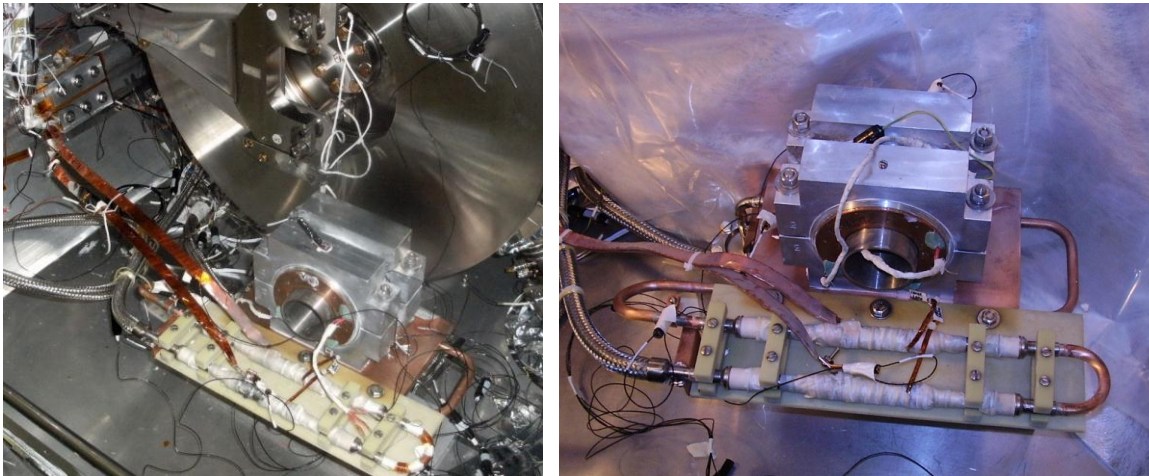


Fig. 11. Photos of the magnet installed in the cryostat

V. Temperature measurements in the magnet #2

In Table 9, the results of the magnet temperature measurements in the inner layer, in the outer layer, and on the top of the clamp are shown made with different current settings of the heater. At each setting of the heater current, the magnet quench current was also measured; the results of the measurements are summarized in Fig. 12 (red squares) and compared with the quench current predicted by Fig. 7 (blue diamonds). Power of the heater for each heater setting is

shown by the purple circles. As one can expect, at higher power of the heater, the temperature of the winding is higher, and the quench current is lower.

Table 9. Temperatures recorded by the sensors installed on the coil at different heater currents

I_heater [mA]	P [mW]	T_in [K]	T_out [K]	T_clamp [K]
0	0	5.24	5.11	5.24
30	16.2	5.54	5.34	5.41
50	45	6.01	5.68	5.66
70	88.2	6.7	6.14	5.99
86.6	135.0	7.38	6.67	6.37
100	180	7.96	7.06	6.69

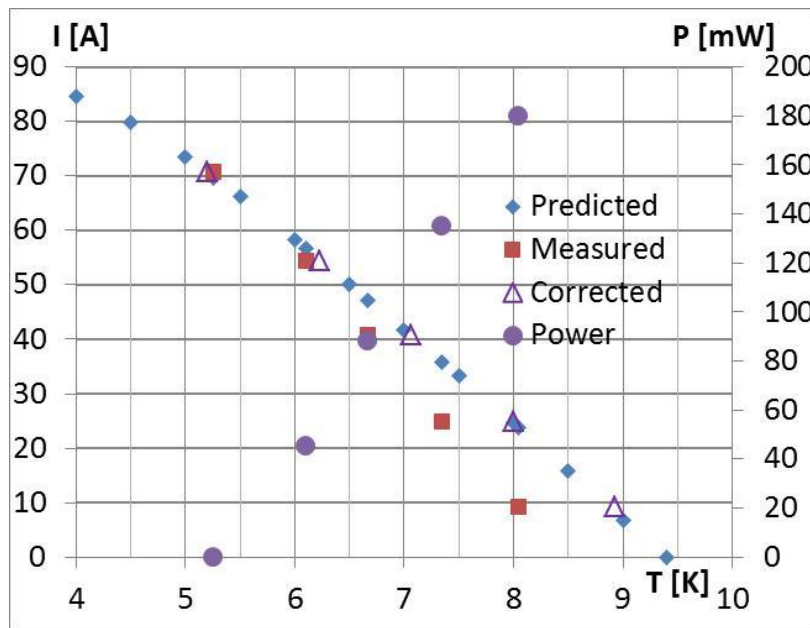


Fig. 12. Quench current corresponding to different readings of the Cernox sensor in the inner layer of the test magnet

A significant departure from the expected strand performance is quite noticeable in Fig. 12. This inconsistency is due to the fact that the temperature sensor in the first layer of the winding is spatially separated from the heater, as was mentioned earlier (see Fig. 6). A correction to the measured temperature of the strand must be applied that would connect the temperature in the quenching spot, which is near one (or several) of the heaters (if they are activated), with what was measured by the sensor. In Fig. 12 this is made by artificially increasing the readings of the sensor; the corrected points are marked by triangles. Fig. 13 plots the correcting temperature rise ΔT against the heater power; the dependence is linear, as it should be expected.

The temperature data shown in Table 3 is also visualized in Fig. 14. When the heater power is higher than ~40 mW, the temperature in the coil exceeds that of the top part of the clamp. Lower temperature of the outer layer reflects the presence of the aluminum compression ring that shunts part of the heat flux from the heaters down to the lower portion of the clamp.

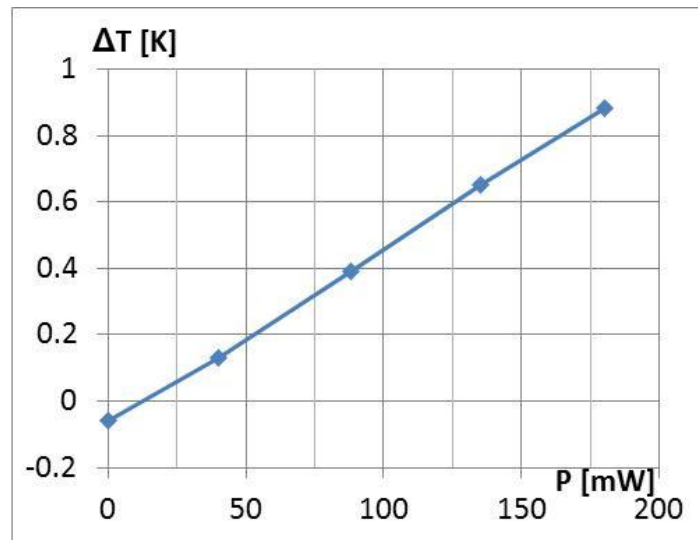


Fig. 13. Correcting temperature difference as a function of the heater power.

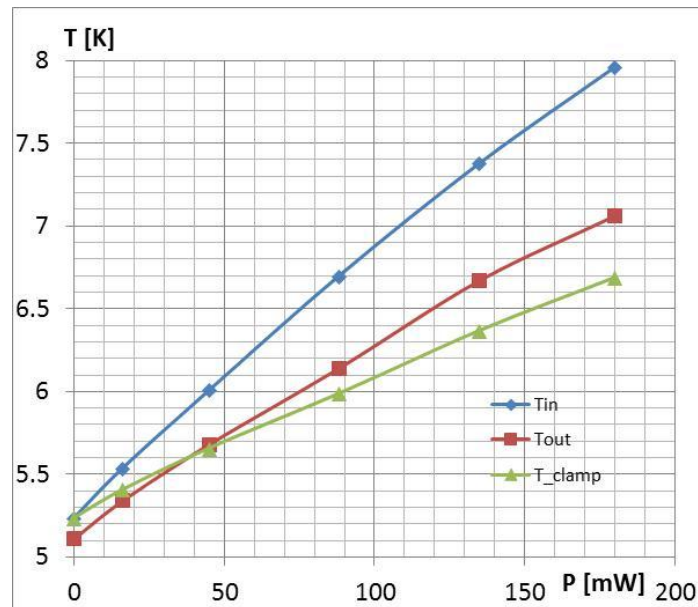


Fig. 14. Readings of the sensors installed on the test coil #2 as functions of the heater power.

At zero heater power, the measured temperature on the top of the clamp is ~ 5.2 K, and there is a difference of ~ 0.5 K between this temperature and the temperature of the heat sink plate, which was ~ 4.7 K and nearly independent of the heater power. So, even when the heaters are not activated, there must be a significant heat flux directed towards the base plate of the assembly through the clamp. The heat responsible for this temperature rise can be delivered to the top of the clamp by copper thermal shields installed near the ends of the coil and connected to the top half of the clamp (see Fig. 6). The temperature dependence on the heater power for the top of the clamp can be approximated by the expression:

$$T(P) = T_{\text{base}} + dT/dP \cdot (P_{\text{heater}} + P_{\text{flux}}).$$

With known P_{heater} , T_{base} , and the temperature measured at each heater current setting $T(P)$, we can obtain the slope of the $T(P)$ curve from the graph in Fig. 21 to find

$$P_{\text{flux}} = 1/(dT/dP) \cdot (T_{\text{clamp}} - T_{\text{base}}) - P_{\text{heater}}$$

The results of corresponding calculation ($dT/dP \approx 8.5 \cdot 10^{-3}$ K/mW) are shown in Table 4. We see a constant heat influx of ~ 65 mW to the top portion of the clamp, which results in its higher temperature and corresponding elevated temperature of the winding.

Table 4. Heat influx to the top of the clamps

P_{heater} [mW]	0	16	45	88.2	135	180
P_{flux} [mW]	64	67	68	63.5	61.5	55.3

By comparing the readings of Cernox sensors installed in the inner and the outer layers of the test magnet #2, we can evaluate the heat flux directed radially outward inside the winding. Thermal resistance of the coil winding (that is $\Delta T/P$) is defined by the material properties and should be the same for any heater power setting; using direct temperature measurements by the sensors embedded in the winding of the test magnet, we see quite a different pattern (Table 5).

Table 5. Observed thermal resistance at different levels of the heater power

P_{heater} [mW]	16	45	88	135	180
$\Delta T/P$ [K/mW]	0.0125	0.0073	0.0064	0.005	0.005

To explain the results of the measurements, we need to assume the existence of an additional heat flux of ~ 20 mW, which is not associated with the heaters, comes into the inner layer of the coil, and propagates radially outward. Taken into account, this additional flux modifies the values of the thermal resistance in Table 5, which become almost independent on the heater power: $\Delta T/P \approx 0.005$ K/mW.

One of the sources of this heat flux could be poor vacuum in the test cryostat. Nevertheless, corresponding estimate resulted in a conclusion that the vacuum level in the cryostat must be much worse than we can assume ($\sim 2 \cdot 10^{-2}$ Pa, or $\sim 2.6 \cdot 10^{-4}$ tor) to explain the data. No reliable data on the vacuum condition in the cryostat exists, unfortunately.

Another source of the heat influx can be thermal radiation due to inadequate amount of MLI material used around the test coil to shield it from the ~ 90 K nitrogen shield radiation (or poor usage of the existing insulating layers). It becomes obvious that one needs to pay significant attention to the quality and proper installation of any shielding.

VI. Temperature of the magnet measured with re-configured radiation shield.

To clarify the source of additional heat flux into the coil, the setup of the test coil was rearranged to redirect the heat flux getting to the top of the clamps through the radiation shield plates in the setup shown in Fig. 6 to the base plate in the setup in Fig. 15. Several layer of the MLI material were also added to the existing MLI blanket to improve the shielding against thermal radiation.

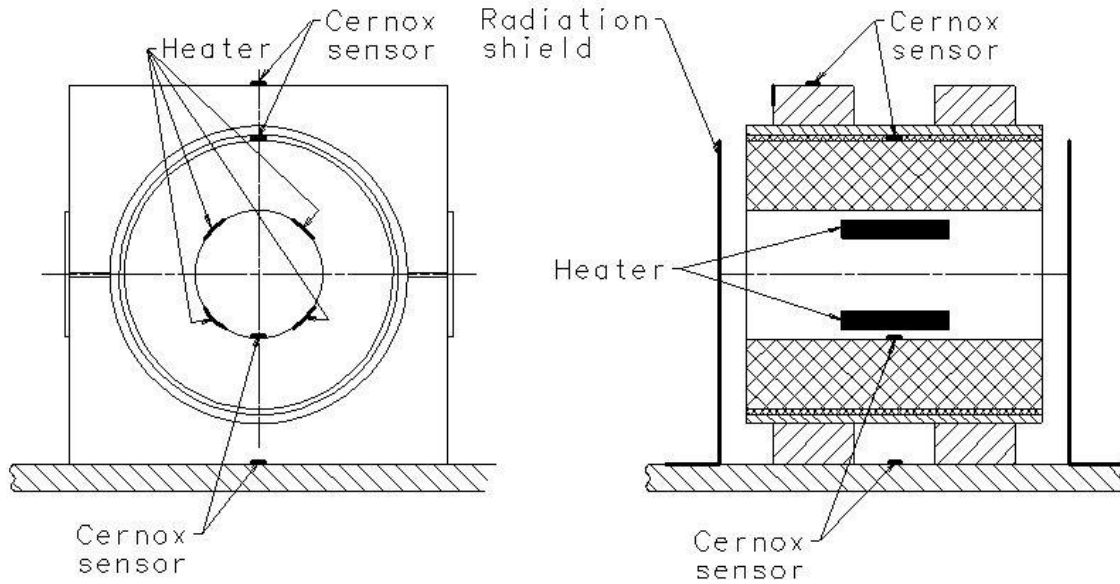


Fig. 15. Test magnet #2 with reconfigured radiation shield.

Table 6 shows temperature recorded at different currents in the heater.

Table 6. Temperatures recorded by the sensors installed on the coil at different heater currents

I_heater [mA]	P [mW]	T_in [K]	T_out [K]	T_clamp [K]	T_base [K]
0	0	4.74	4.67	4.98	4.57
30	16.2	5.02	4.83	5.1	4.60
50	45	5.47	5.16	5.3	4.60
70	88.2	5.99	5.55	5.55	4.63
86.6	135.0	6.61	5.89	5.78	4.63
100	180	7.13	6.24	5.98	4.63
120	253	8.0	6.86	6.4	4.63

The same set of data is plotted in Fig. 16.

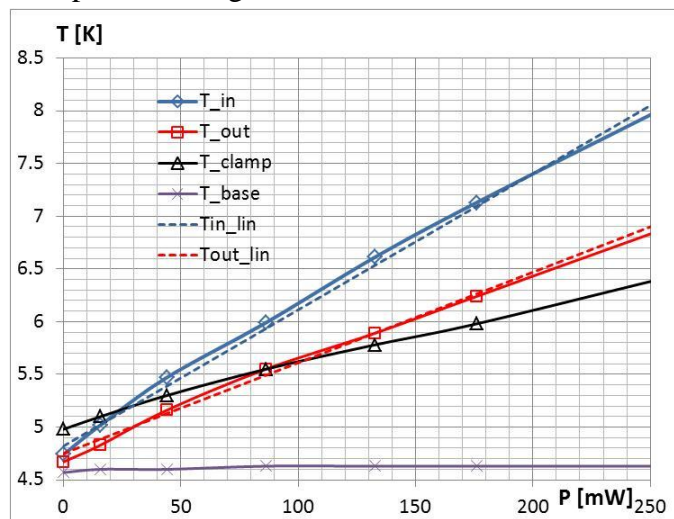


Fig. 16. Temperatures in the setup with the radiation shields connected to the base plate.

Temperature of the coil (the inner and the outer layers) now is significantly (~ 0.5 K) lower. With the heaters off, the temperature on the top of the clamp is higher than the temperature in the area where the inner layer sensor is installed (Fig. 6); this tells us that the temperature in the inner layer is not uniform – it is higher in the part which is farther from the heat sink. This means that a significant heat flux comes to the heat sink plate through the clamp and compression ring.

As was done earlier, the next expression will be used to evaluate this flux:

$$P_{\text{flux}} = 1/(dT/dP) \cdot (T_{\text{clamp}} - T_{\text{base}}) - P_{\text{heater}}$$

By using the clamp temperature curve in Fig. 16, we can find the thermal resistance at small values of the heater power P : $dT/dP \approx 0.007$ K/mW. It is a bit lower than in the previous case, which indicated better thermal flow arrangements made this time. Since we also know the temperature of the base (see Table 6), we can calculate values of the unknown heat flux for any setting of the heater; results of the calculation are shown in Table 7.

Table 7. Environmental heat flux into the test coil

P_{heater} [mW]	0	16	45	88.2	135	180	253
P_{flux} [mW]	73	73	75	78	72	65	63

The heat flux to the clamp and the outer surface of the coil is quite comparable with what was found in the previous test setup (see Table 4 and corresponding comments). The difference between the two settings is some rearrangement of the way this flux reaches the heat sink.

The value of the heat flux to the inner surface of the coil can also be found by using the information in Table 6. For temperature traces in Fig. 16, we will use linear approximations of the temperature dependence on the heater power (corresponding lines are shown in Fig. 16 as dashed lines):

$$T_{\text{in_lin}} \text{ [K]} = 4.82 + 0.0129 \cdot P[\text{mW}]$$

$$T_{\text{out_lin}} \text{ [K]} = 4.75 + 0.0086 \cdot P[\text{mW}]$$

By solving the equation $T_{\text{in_lin}} = T_{\text{out_lin}}$, we can find the temperature corresponding to the zero total heat flux, and the value of the parasitic heat flux (not associated with the heaters): $T_0 = 4.61$ K and $P_0 = 16.3$ mW. As expected, the crossing temperature is close to the temperature of the heat sink plate, which was changing during the test between 4.58 K and 4.63 K (see Table 6).

Because, the temperature in the magnet winding is not uniform, it is important to relate the magnet performance with readings of the sensor installed on the inner surface of the coil. Fig. 22 shows the measured quench current (red squares) at different settings of the heater power (green crosses) related to the temperature registered by the sensors. As we have already learned, the readings of sensors embedded in the coil do not provide correct information about the hottest spot in the coil; we need to use correction obtained from Fig. 13. The reading of the sensor in the inner layer must be increased by $\Delta T \text{ [K]} = 0.005 \cdot P \text{ [mW]}$, where P is the heater power. For example, for $P = 100$ mW, the temperature correction is 0.5 K. This temperature correction leads to the correction in the quench current calculated based on the measured temperature:

$$\Delta I = (dI/dT) \cdot \Delta T,$$

where dI/dT is found as a slope of the linear part of the strand performance curve (~ 17 A/K). The adjusted values are shown as circles in Fig. 17 for several heater power values; they are in good agreement with the expected strand performance. This agreement shows that the temperature readings by the Cernox sensors can be trusted.

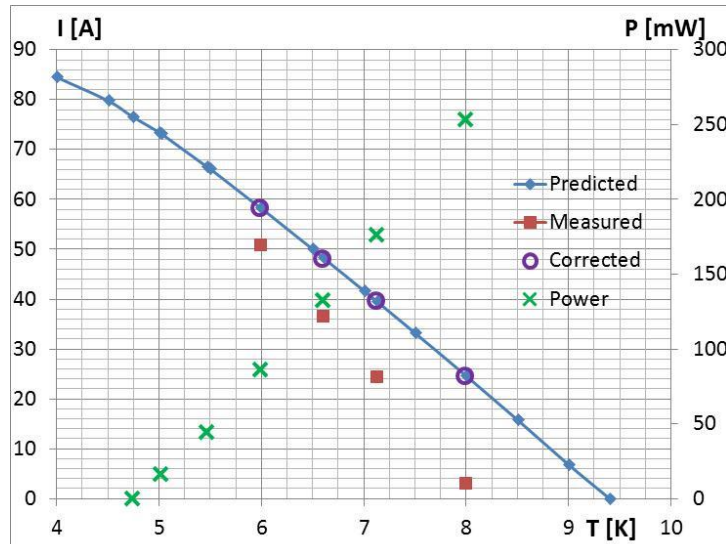


Fig. 17. Quench current at different settings of the heater power compared with the strand performance.

VII. Summary

As a result of the study of feasibility of using conduction cooling in the cryomodules of linacs, we can state the following:

1. Performance of the conduction-cooled systems is defined by properties of the strand and the temperature of the winding, which is quite susceptible to even small heat influxes.
2. For the test coils used during this R&D the heat flux to the inner surface of the test coil was ~ 20 mW, which was enough to elevate the winding temperature by ~ 0.2 K.
3. To reduce the difference of the temperature inside the winding, it is important to make thorough thermal design of the system to minimize thermal resistance from the coil to the heat sink.
4. As the temperature of the conductively-cooled winding could be made just 0.2 K higher than that of the heat sink, using conduction cooled superconducting magnetic systems in cryomodules of superconducting linacs seems quite feasible.

References:

1. S. Nagaitsev, "PXIE Overview: Goals, Concepts, and Planning", Project X-doc-1025-v1 09 Apr 2012.
2. Madrak, et al, "First High Power Pulsed Tests of a Dressed 325 MHz Superconducting Single Spoke Resonator at Fermilab", PAC-2011.
3. S. Cheban, et al, "Conductively Cooled Current Leads for Use in the SSR1 Test Cryostat", FNAL TD note TD-12-004.
4. I. Terechkine, "Test Solenoid Design Proposal", TD-05-040, Sept. 23, 2005.
5. R. Carcagno, et. Al, "Test Solenoids. Expected Performance and Test Results", TD-06-027, July 21, 2006.
6. K.-H. Mess, P. Schmuser, S. Wolff, Superconducting Accelerator Magnets, World Scientific, 1996, p. 196
7. G.K. White, P.J. Meeson, Experimental Techniques in Low Temperature Physics, Clarendon, Oxford, 2002.